Sideslip Effects on Fin-Fin Interference in Supersonic Missile Aerodynamics

A. A. Jenn*
McDonnell Douglas Astronautics Company, St. Louis, Missouri
and
H. F. Nelson†
University of Missouri—Rolla, Rolla, Missouri

The supersonic missile fin-fin interference factor K_ϕ is a measure of the normal force change on a fin, in the presence of a body and other fins, caused by changes in sideslip angle. A finite-difference Euler code, SWINT, is used to numerically determine the fin forces for different sideslip angles for two-, three-, four-, and six-fin missile configurations at small angles of attack. The fin forces are used to evaluate K_ϕ at Mach numbers from 2.5–3.5, positive and negative sideslip angles, and various fin aspect ratios. The K_ϕ values from SWINT for two-fin configurations have similar magnitudes to those from previously published slender body theory analytical solutions; however, the SWINT predictions for four-fin configurations show that K_ϕ breaks away sharply from the slender body theory values as the fin span increases. The fin span at which the breakaway occurs is shown to be directly related to the position of shock waves and expansion fans originating from neighboring fins. The breakaway fin span is also shown to be a strong function of the number of fins, Mach number, and sideslip angle. Values of K_ϕ for use in preliminary design are presented.

Nomenclature

$\mathcal{R}$	= aspect ratio of wing formed by joining two fins
B	= Mach number parameter $= \sqrt{M_\infty^2 - 1}$
$(C_N)_F$	= fin normal force coefficient referenced to fin area
$(\Delta C_N)_F$	= change in fin normal force coefficient due to sideslip
$(C_N)_W$	= normal force coefficient on wing alone formed by joining two fins
D	= body diameter
$K_{W(B)}$	= wing-body interference factor due to upwash
K_ϕ	= fin-fin interference factor due to sideslip
M_∞	= freestream Mach number
P_∞	= freestream pressure
R	= body radius
S	= fin span measured from body centerline
SBT	= slender body theory
S/R	= fin span to body radius ratio
Z	= missile axial coordinate measured from nose
Z_F	= fin axial location on missile
α	= missile angle of attack
α_F	= fin angle of attack
α_{eq}	= equivalent angle of attack
$(\Delta\alpha_{eq})_v$	= induced change in angle of attack due to vortices
β	= missile sideslip angle
β_F	= fin sideslip angle
ϵ	= fin semivertex angle
ϕ_F	= fin roll angle

Received Dec. 4, 1987; presented as Paper 88-0214 at the AIAA 26th Aerospace Sciences Meeting, Reno, NV, Jan. 11–14, 1988; revision received May 19, 1988.

*Engineer, Aeromechanics Department. Member AIAA.
†Professor of Aerospace Engineering, Thermal Radiation Transfer Group, Department of Mechanical and Aerospace Engineering. Associate Fellow AIAA.

Introduction

A FAST and simple method of predicting the aerodynamic interaction between missile fins is important for preliminary design. The complex flowfield surrounding a finned vehicle in supersonic flight[1-3] is governed by nonlinear partial differential equations. Numerical methods that will solve these or simplified versions of these equations are available,[4-5] but often require a great deal of user expertise and computer time, which both translate into increased cost. Currently, component buildup methods[6-8] offer a fast and economical way of determining preliminary design parameters such as force and moment coefficients and stability derivatives. A specific component buildup technique used for missile fins is the equivalent angle-of-attack method. It models the nonlinear lifting characteristics of missile fins by defining the equivalent angle of attack as

$$\alpha_{eq} = K_{W(B)}\alpha_F + \frac{4}{\mathcal{R}} K_\phi \alpha_F \beta_F + (\Delta\alpha_{eq})_v \tag{1}$$

where the terms on the right-hand side represent contributions due to body upwash, fin sideslip angle, and vortex interaction, respectively. The equivalent angle-of-attack method is derived and its accuracy demonstrated in Ref. 9. Extensions of the method to high angles of attack are discussed in Refs. 10 and 11.

The purpose of this research is to investigate the effect of sideslip angle on fin normal force. This effect is characterized by K_ϕ in Eq. (1), which is defined as

$$K_\phi = \frac{(\Delta C_N)_F}{(C_N)_W} \frac{\tan\epsilon}{\beta_F} \tag{2}$$

Here, K_ϕ is an explicit function of β_F, or an implicit function of ϕ_F since for zero sideslip and small angles of attack,

$$\alpha_F = \alpha\cos\phi_F$$
$$\beta_F + \alpha\sin\phi_F \tag{3}$$

$(\Delta C_N)_F$ represents the change in fin loading due to sideslip angle and is determined from the difference in fin normal

force coefficient between a fin at $\beta_F \neq 0$ and a fin at $\beta_F = 0$ as

$$(\Delta C_N)_F = (C_N)_{F_{\substack{(\beta \neq 0)\\(\alpha = \alpha)}}} - (C_N)_{F_{\substack{(\beta = 0)\\(\alpha = \alpha)}}} \tag{4}$$

The parameters $(C_N)_W$ and $\tan\epsilon$ are used to normalize the K_ϕ values. For triangular fins, ϵ is related to $\mathcal{R}$ by

$$\mathcal{R} = 4\tan\epsilon \tag{5}$$

K_ϕ was evaluated by Nielsen[12] for planar and cruciform fin configurations. Nielsen predicted values of K_ϕ for triangular fins as a function of S/R and number of fins using slender body theory (SBT). According to SBT, $(\Delta C_N)_F$ is proportional to β_F; thus, Nielsen's results for K_ϕ are independent of the fin sideslip angle. His analysis was limited to two- and four-fin missile configurations and the results are shown in Fig. 1.

Slender body theory is a special case of linearized potential theory. It can be derived directly from the full potential equation.[13] Slender body theory can also be derived by assuming that the axial flow derivatives are small compared to the crossflow derivatives and, therefore, can be neglected. This reduces the flow problem to Laplace's equation in the crossflow plane with a time-varying boundary condition. These simplifications preclude the modeling of shock waves in the flow and also limit the analysis to small angles of attack and sideslip.

Analytical Methodology

The methodology used in this research to determine K_ϕ follows that used by Nielsen in Ref. 12. He used slender body theory to analytically determine changes in the fin pressure distribution due to sideslip angle. The incremental pressure distribution was integrated for triangular fins to determine $(\Delta C_N)_F$ for the entire range of S/R. Equation (2) was then used to determine K_ϕ.

The primary difference between this research and Nielsen's analysis is in the theoretical model used to determine fin loading. A numerical Euler code, SWINT,[14] was employed for this research. SWINT uses a finite-difference axial marching scheme in a supersonic flow domain bounded by the body and the bow shock. The fins are modeled as discontinuities in the solution domain using a thin fin approximation. The conservation equations are cast in conservative form, allowing shock waves to be captured by the numerical scheme. Exact boundary conditions are used whenever possible; however, empirical boundary conditions are used when phenomena such as subsonic fin leading edges or body-wing root junctions are encountered. The computation is started by specifying an initial data plane near the nose of the body. The flowfield solution is advanced by marching axially along the missile body. SWINT predictions have been shown to agree well with both experimental data and other numerical results for a wide variety of missile configurations and flight conditions.[15-16] SWINT was modified slightly for this research to separately calculate the normal forces on each fin. This was necessary to determine K_ϕ.

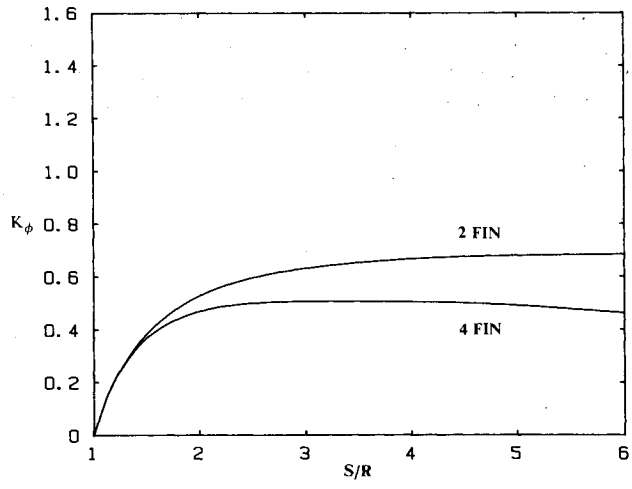

Fig. 1 K_ϕ vs fin span for planar and cruciform fin configurations from slender body theory.

Missile Geometry

The missile configuration selected for the SWINT runs had a conical nose with a length-to-diameter ratio of 3 and a cylindrical body. The fins were infinitely thin flat plates with triangular planforms. Missile configurations with two, three, four, and six equally spaced fins were used, and in each case, the fins were oriented around the body such that at least one fin was positioned horizontally ($\phi_F = 0$). This fin was used for the K_ϕ analysis since $\alpha_F = \alpha$ and $\beta_F = \beta$ for small values of α and β. Figure 2 shows the missile geometry and the different fin set arrangements.

K_ϕ was found to be sensitive to fin location Z_F in regions of varying pressure along the body. In order to determine K_ϕ independent of Z_F, it was necessary to investigate the pressure distribution along the body with no fins. Figure 3 shows the SWINT predictions for the body pressure distribution as a function of axial and circumferential location at $M_\infty = 3$ and 4 with $\alpha = 3$ deg and $\beta = 0$. The effects of the flow expansion caused by the cone-cylinder junction are apparent far aft of the nose, resulting in the sensitivity of K_ϕ to changes in Z_F. In order to reduce the sensitivity of K_ϕ to Z_F, the fins were located at $Z_F/D = 16$ where the pressure is relatively constant along the body.

The pressure variations along the body are indicative of the axial pressure variations in the entire flowfield. Thus, when a fin is located at a point on the body where the pressure is varying, changes in Z_F will result in small changes in $(C_N)_F$. This, in turn, affects $(\Delta C_N)_F$; however, since $(\Delta C_N)_F$ is usually less than 5% of $(C_N)_F$, the small changes in $(C_N)_F$ can cause very large changes in $(\Delta C_N)_F$. K_ϕ, being directly proportional to $(\Delta C_N)_F$, is thus highly sensitive to changes in the fin normal force caused by the pressure variations in the flowfield.

Force Normalization

K_ϕ is determined by normalizing $(\Delta C_N)_F$ with the wing-alone normal force coefficient $(C_N)_W$ as shown in Eq. (2). Ideally, SWINT would be used to determine $(C_N)_W$ by computing the normal force on a wing composed of two fins joined together at their root chords at $\beta = 0$ deg. SWINT, however, assumes that the fins lie entirely within the missile

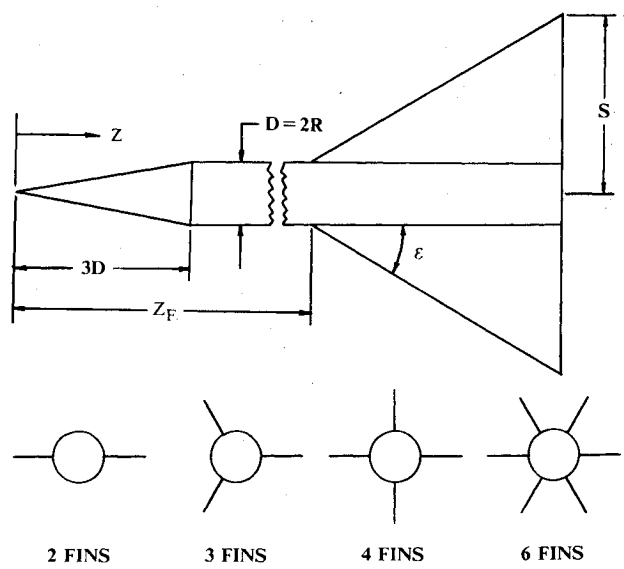

Fig. 2 Missile and fin configurations.

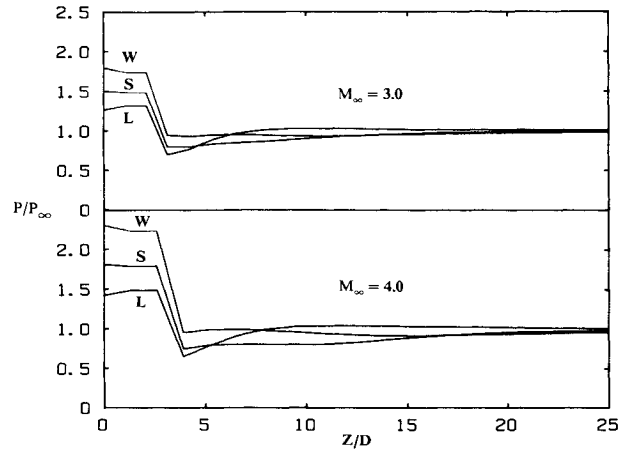

Fig. 3 Body-alone pressure distribution at $M_\infty = 3$ and 4 for $\alpha = 3$ deg and $\beta = 0$ deg (L = leeside, W = windward, S = side).

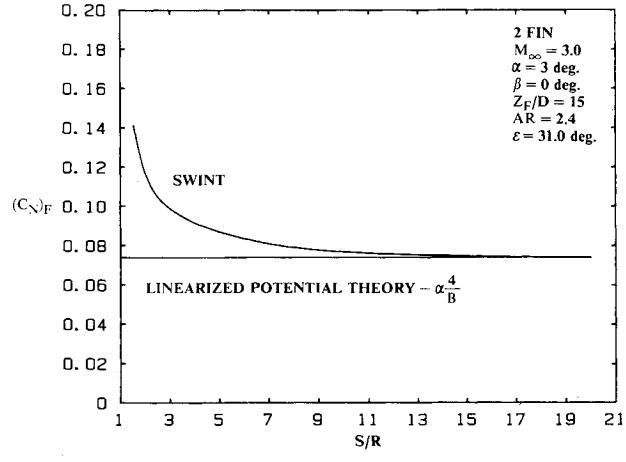

Fig. 4 Comparison of $(C_N)_F$ from SWINT for fin in presence of body and $(C_N)_W$ from linearized potential theory for fin alone as a function of fin span.

bow shock; therefore, a wing-alone case cannot be analyzed. Consequently, linearized potential theory was used to determine $(C_N)_W$. For a wing alone with supersonic leading edges,

$$(C_N)_W = 4\alpha/B \tag{6}$$

Equation (6) was used to determine $(C_N)_W$ for all cases since fins with subsonic leading edges were not considered here. A missile with large fins ($S/R = 20$) was analyzed using SWINT to check SWINT predictions against linearized potential theory as shown in Fig. 4. As the fins become large relative to the body, $(C_N)_F$ predicted by SWINT asymptotically approaches $(C_N)_W$ predicted by linearized potential theory. This shows that the use of Eq. (6) to determine $(C_N)_W$ does not compromise the results of the K_ϕ analysis.

Data Reduction

A computer program was written to convert fin normal force data from SWINT into tabulated K_ϕ values.[17] Typical SWINT output gives normal force data at 40 to 60 different axial locations along the missile fin. Two calculations, one at $\beta = 0$ and one at $\beta \neq 0$, are needed to evaluate $(\Delta C_N)_F$; however, each SWINT calculation yields data at slightly different fin axial locations. The data reduction program first converts the normal force data to nondimensional coefficient form as shown in Fig. 5. The two curves shown in Fig. 5 are for $\beta = 0$ and 3 deg, and the difference between the curves represents $(\Delta C_N)_F$. Four-point Lagrange interpolation is then

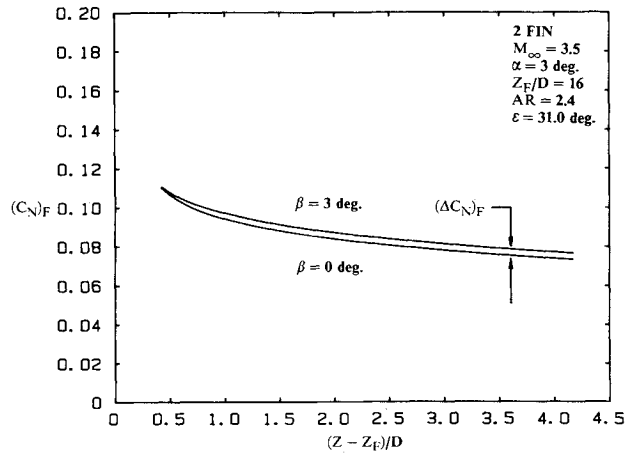

Fig. 5 Comparison of $(C_N)_F$ on a missile fin at $\beta = 0$ and 3 deg as a function of root chord length for a two-fin missile configuration.

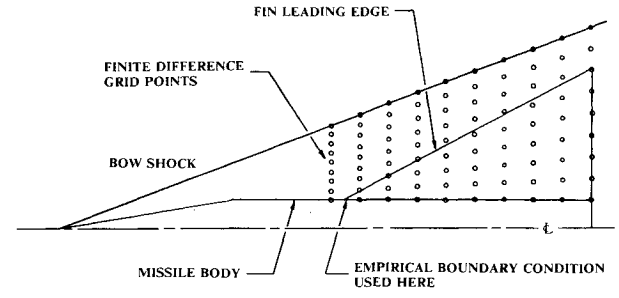

Fig. 6 SWINT finite-difference grid distribution on a horizontal fin surface.

used to determine $(C_N)_F$ for each sideslip angle at evenly spaced increments along the fin. Subsequently, $(\Delta C_N)_F$ is determined using Eq. (4). Each value of $(\Delta C_N)_F$ is used to determine K_ϕ for a specific value of S/R. This is possible because the flow over the fin is supersonic so that downstream flow phenomena do not affect upstream results. The value of S/R is related to axial location along the fin and ϵ as

$$\frac{S}{R} = \frac{(Z - Z_F)}{R}\tan\epsilon + 1 \tag{7}$$

K_ϕ data generated at $S/R < 3$ often showed trends that were not consistent with the results of SBT shown in Fig. 1. Often, K_ϕ fluctuated randomly for $S/R < 2$ because the SWINT predictions for $(C_N)_F$ are not accurate for small fins. This occurs for the following reasons. First, for $S/R < 3$, the fin span is small compared to the radial distance between the body and bow shock. SWINT uses a finite-difference mesh with evenly distributed grid points between the body and bow shock as shown in Fig. 6. This leads to a relatively small number of grid points that actually fall on the fin, resulting in reduced accuracy for the normal force calculation on small fins. Second, SWINT employs an empirical correlation to handle the body-wing root junction. This leads to additional error that is significant for small fins. Third, K_ϕ is a function of $(\Delta C_N)_F$, and Fig. 5 shows that this difference is small for small fins. This leads to numerical error caused by subtracting two numbers that are nearly identical. As S/R increases beyond 3, a larger number of grid points are located on the fin, and $(\Delta C_N)_F$ increases; therefore, the accuracy of the K_ϕ calculation is increased.

Improved K_ϕ results were obtained for small fins by increasing the number of radial mesh points used by SWINT from 72 to 120. The increased mesh size resulted in K_ϕ val-

ues that agreed well with the SBT data in Fig. 1 down to $S/R = 1.5$.[17] This suggests that one use K_ϕ from SBT for small fins and K_ϕ from SWINT for larger fins to predict K_ϕ over the entire range of S/R. The data-reduction procedure was expanded by scaling the two-fin results for K_ϕ from SBT to match the magnitude of the SWINT K_ϕ data at a specified S/R value between 2 and 3. The value of S/R at which the data were matched was chosen such that the slopes of the two curves were approximately equal. Only the two-fin K_ϕ data from SBT was used since K_ϕ becomes independent of the number of fins at small values of S/R.

Results and Discussion

According to slender body theory, K_ϕ is a function of S/R and the number of fins. The Euler equations, solved by SWINT, are nonlinear, which suggests that additional parameters such as M_∞, α, β, and ϵ could also influence K_ϕ. The results presented here focus primarily on the effects of S/R, the number of fins, M_∞, and ϵ. Sideslip angle effects are discussed, but only for $\beta = \pm 3$ deg. The values of α and β were kept small and proved to have little or no effect on K_ϕ.[17]

The use of SWINT was kept as simple as possible for these predictions. No mesh clustering or smoothing options were used. The flowfield solution was determined for the entire 360 deg around the missile. This was necessary since no pitch plane symmetry exists for $\beta \neq 0$. The computational mesh was refined three times between the nose and the finned section of the missile in order to reduce computer run times. A 20×20 mesh was used for $Z/D < 5$. This was increased to a 40×40 mesh for $Z/D < 10$, a 60×60 mesh for $Z/D < 15$, and finally, a 72×72 mesh for the flowfield over the finned section of the vehicle.

Sideslip Angle and Mach Number Effects

The effect of positive and negative sideslip angles on K_ϕ was investigated for $M_\infty = 2.5$, 3.0, and 3.5. The sideslip angles used were $\beta = \pm 3$. These results are shown in Figs. 7–12 and summarized in Fig. 13. The dashed line represents the scaled two-fin results from SBT in these figures. It covers the S/R region where the SWINT results were inaccurate.

Figure 7 shows K_ϕ for each fin configuration at $M_\infty = 2.5$, $\epsilon = 45.0$ deg and $\beta = 3$ deg. The two-fin results are similar to the slender body theory results for K_ϕ shown in Fig. 1. The three-fin K_ϕ curve is identical to the two-fin curve for all values of S/R shown. This occurred for every case considered in this research. As the number of fins is increased beyond three, K_ϕ breaks away sharply from the two-fin value. The breakaway point occurs at $S/R = 4.6$ for the four-fin case and $S/R = 3.2$ for the six-fin case. Below $S/R = 3.2$, K_ϕ for each fin configuration is the same.

Figure 8 shows the same data as Fig. 7 except $\beta = -3$ deg. The variation of K_ϕ is similar to that for $\beta > 0$, except for slightly larger magnitudes. In addition, the S/R values at which the four- and six-fin results breakaway from the two-fin results are lower than the breakaway values for $\beta > 0$.

Figures 9 and 10 show K_ϕ at $M_\infty = 3.0$ and $\epsilon = 38.7$ deg, whereas Figs. 11 and 12 show K_ϕ at $M_\infty = 3.5$ and $\epsilon = 31.0$ deg. The fin semivertex angle was decreased to keep the four-fin breakaway point from moving beyond $S/R = 6$. The sideslip angle is 3 deg in Figs. 9 and 11 and -3 deg in Figs. 10 and 12. In each case, the K_ϕ results are similar to the $M_\infty = 2.5$, $\epsilon = 45.0$ deg results of Figs. 8 and 9 for the given sideslip angle.

Figures 7–12 show that K_ϕ is generally larger for $\beta < 0$ than for $\beta > 0$. Also, the breakaway S/R values for the four- and six-fin cases are lower for $\beta < 0$. The Mach number effects on K_ϕ are not easily determined from Figs. 7–12 since ϵ was varied along with M_∞. The effect of M_∞ on K_ϕ was determined for $2.75 \leq M_\infty \leq 4.00$ with ϵ held constant at 31.0 deg. The breakaway S/R values for the four- and six-fin cases are shown in Fig. 13 for $\beta = \pm 3$ deg. This figure shows the maximum value of S/R for which the two-fin K_ϕ is equal to K_ϕ for four or six fins. For example, at $M_\infty = 3.0$ and $\beta = 3$ deg, a missile with four fins has the same K_ϕ as a missile with two fins for $S/R < 3.7$. At $S/R > 3.7$, the four-fin K_ϕ differs from the two-fin K_ϕ. As M_∞ is increased, the breakaway values of S/R increase for both the four- and six-fin configurations at both sideslip angles.[17]

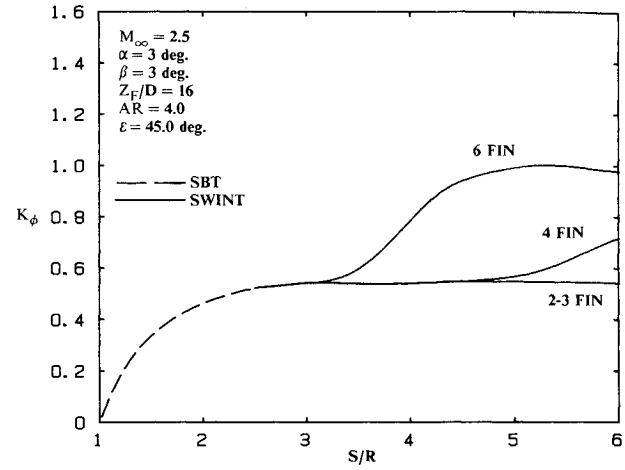

Fig. 7 K_ϕ vs fin span for $M_\infty = 2.5$ and $\beta = 3$ deg.

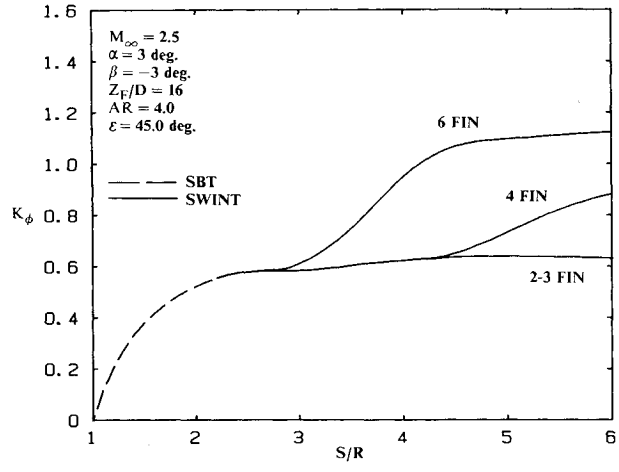

Fig. 8 K_ϕ vs fin span for $M_\infty = 2.5$ and $\beta = -3$ deg.

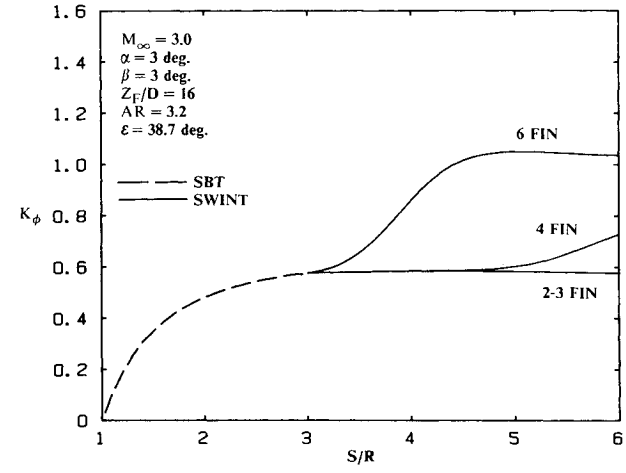

Fig. 9 K_ϕ vs fin span for $M_\infty = 3.0$ and $\beta = 3$ deg.

Semivertex Angle Effects

The effect of semivertex angle on K_ϕ is shown in Figs. 9 and 14–16. Figures 14, 9, and 15 show K_ϕ at $M_\infty = 3.0$ and $\beta = 3$

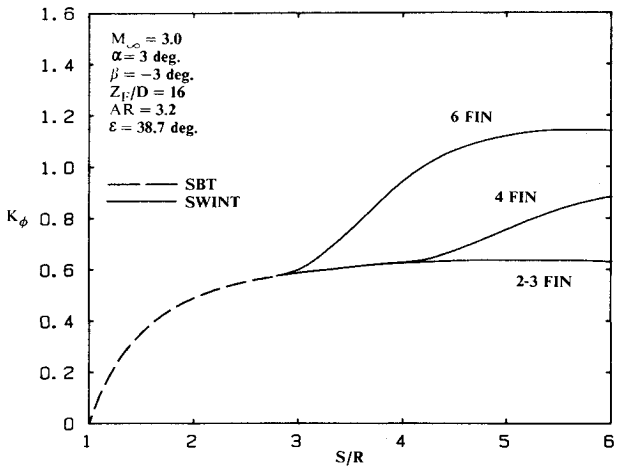

Fig. 10 K_ϕ vs fin span for $M_\infty = 3.0$ and $\beta = -3$ deg.

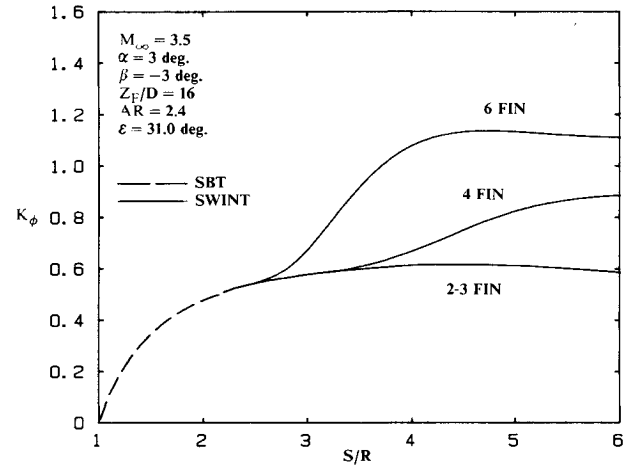

Fig. 11 K_ϕ vs fin span for $M_\infty = 3.5$ and $\beta = 3$ deg.

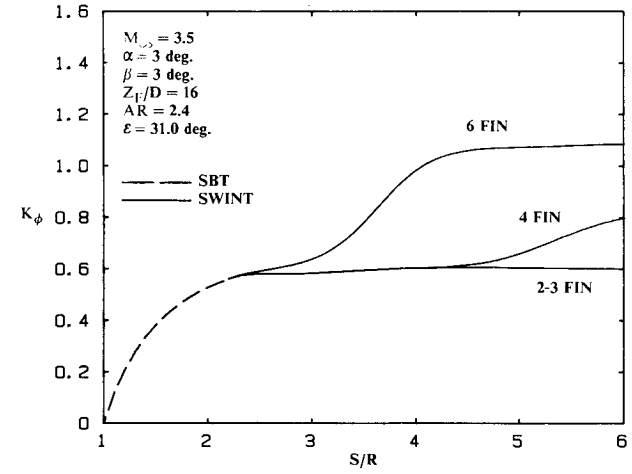

Fig. 12 K_ϕ vs fin span for $M_\infty = 3.5$ and $\beta = -3$ deg.

deg for $\epsilon = 31.0$, 38.7, and 45.0 deg, respectively. The effect of increasing ϵ is similar to that of increasing M_∞. As ϵ increases, the two-fin K_ϕ increases slightly, and the breakaway points move to higher values of S/R. Figure 15 shows that for $\epsilon = 45.0$ deg, the two- and four-fin K_ϕ are identical below $S/R = 5.7$. The breakaway values of S/R are illustrated in Fig. 16 as a function of ϵ for four- and six-fins with $\beta = \pm 3$ deg. The effect of increasing ϵ on the breakaway points is similar to the effect of increasing M_∞. As ϵ increases, the

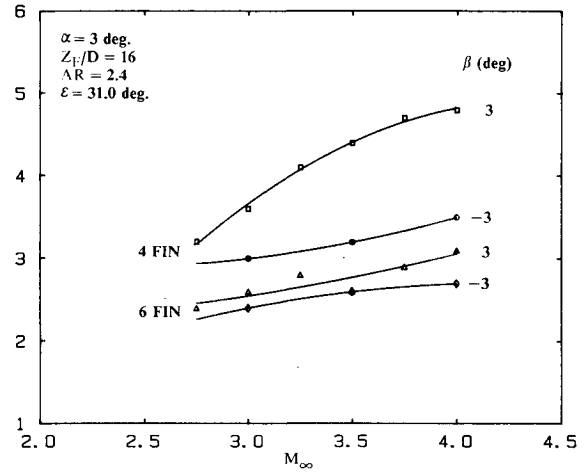

Fig. 13 Effect of Mach number on S/R at which K_ϕ for four- and six-fin configurations breaks away from K_ϕ for two-fin configurations.

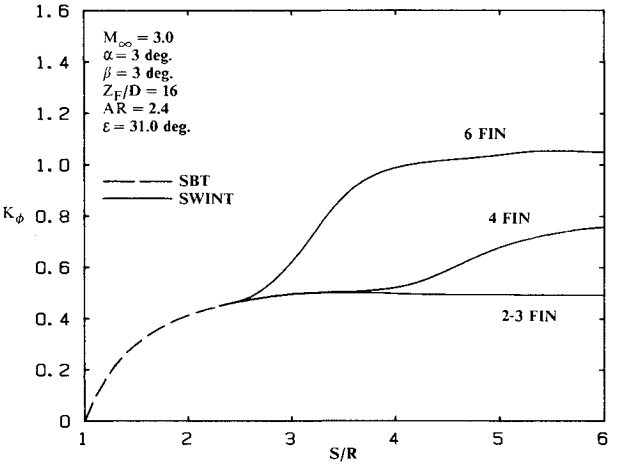

Fig. 14 K_ϕ vs fin span for $M_\infty = 3.0$ and $\epsilon = 31.0$ deg.

breakaway values of S/R also increase for both positive and negative sideslip angles.

Fin Shock Waves and Expansion Fans

K_ϕ values predicted using SWINT are somewhat different than the SBT results. The magnitude of K_ϕ is similar; however, SBT predicts that K_ϕ decreases as the number of fins increases. SWINT pressure predictions on the fins were examined to explain the unexpected trend in K_ϕ. Pressures on the top and bottom of the horizontal fin were compared for two- and four-fin configurations at $\alpha = 3$ deg and $\beta = \pm 3$ deg at $M_\infty = 3.5$. The pressure values near the leading and outboard edge of each fin were identical. Near the inboard trailing edge of the four-fin configuration, the pressures were higher than the two-fin configuration on the top and bottom of the horizontal fin for $\beta = 3$ deg, and lower than the two-fin configuration on the top and bottom of the horizontal fin for $\beta = -3$ deg. Since the only difference between the two- and four-fin configurations is the presence of vertical fins, this suggests that oblique shock waves and expansion fans attached to the vertical fins intersect the horizontal fin and change its pressure distribution. Figure 17 shows an oblique shock wave attached to the lower vertical fin that intersects the bottom of the horizontal fin.

The SWINT results were further analyzed by subtracting the pressures on each surface of the horizontal fin for a two-fin case from the pressures on each surface of the horizontal fin for a four-fin case. The resulting pressure difference contours are shown in Figs. 18 and 19.

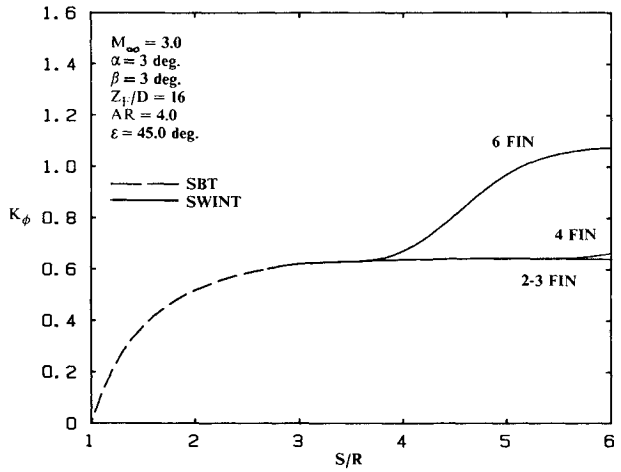

Fig. 15 K_ϕ vs fin span for $M_\infty = 3.0$ and $\epsilon = 45.0$ deg.

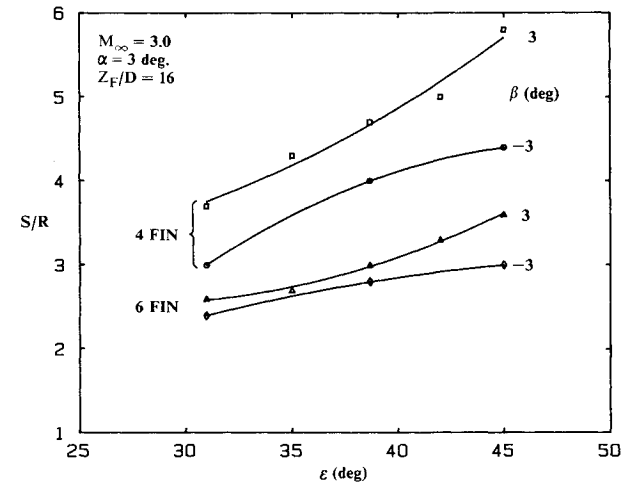

Fig. 16 Effect of fin semivertex angle on S/R at which K_ϕ for four- and six-fin configurations breaks away from K_ϕ for two-fin configurations.

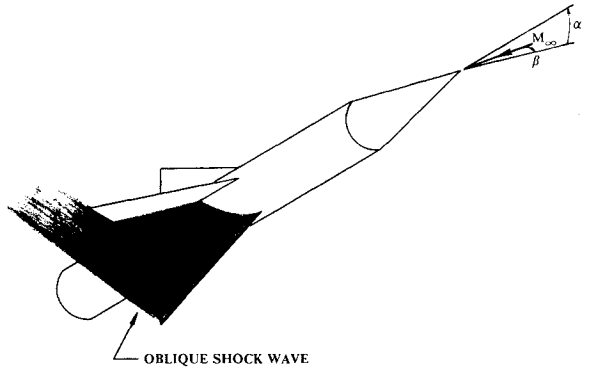

Fig. 17 Fin/shock wave interaction due to positive sideslip on missile with cruciform fin configuration.

Figure 18 shows the regions in which the pressures are different between the two- and four-fin configurations for $\beta = 3$ deg. The pressure begins to increase first on the bottom surface at $S/R = 4.2$. Figure 11 shows that this corresponds to the breakaway value of S/R for the four-fin case. At $S/R = 4.8$, the pressure begins to increase on the top surface. This corresponds to the inflection point in the four-fin K_ϕ data. The increase in pressure for the four-fin case indicates that oblique shock waves intersect the top and bottom surfaces of the horizontal fin. The maximum pressure difference on each surface is 20% of the freestream pressure, but the larger

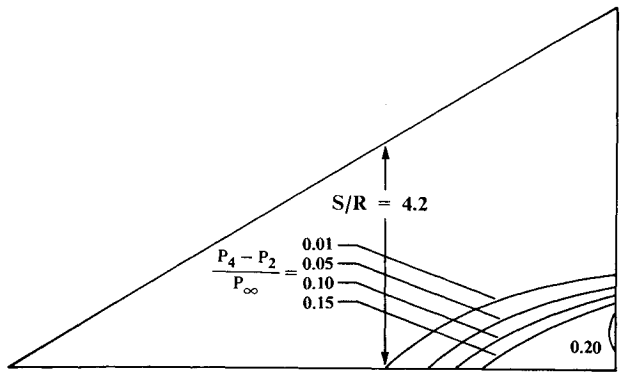

a) Bottom surface, $\beta = 3$ deg

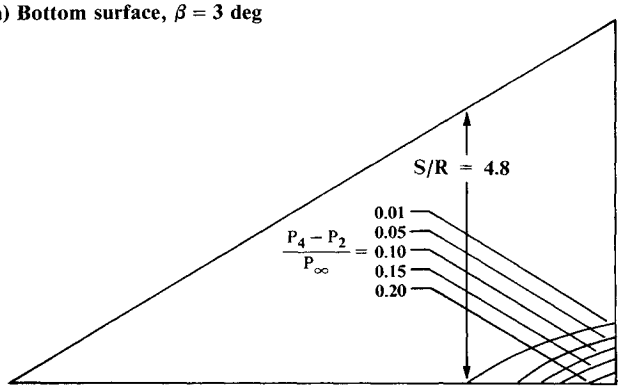

b) Top surface, $\beta = 3$ deg

Fig. 18 Contour plot of fin pressure differences between four- (P_4) and two- (P_2) fin cases at $M_\infty = 3.5$, $\alpha = 3$ deg, $\epsilon = 31.0$ deg, and $\beta = +3$ deg.

fin area covered by the lower fin shock wave causes a net increase in the fin normal force. This leads to the differences in K_ϕ between the two- and four-fin cases.

A similar explanation can be applied to Fig. 19. The negative sideslip angle causes an expansion fan to form on the vertical fins that intersects the horizontal fin, resulting in lower pressure on part of the horizontal fin surfaces for the four-fin configuration relative to the two-fin configuration. The larger fin area affected by the expansion fan on the bottom of the fin leads to a net decrease in the fin normal force, which for a negative sideslip angle, results in an increase in K_ϕ. The breakaway S/R value and the inflection point on the four-fin curve in Fig. 12 correlate with the location of the expansion fans.

A similar analysis was performed with a six-fin missile configuration. The problem is more complex due to shock waves and expansion fans that are present at angle of attack when $\beta = 0$.[17] The vertical fins of the four-fin configuration do not affect the flowfield at $\beta = 0$, even at angle of attack, since they lie along a plane of symmetry in the flow. The additional shock waves and expansion fans present at $\beta = 0$ and $\alpha \neq 0$ must be accounted for when determining the pressure difference between the six- and two-fin cases for $\beta \neq 0$.

The formation of shock waves and expansion fans that intersect the missile fins is consistent with the trends in the K_ϕ data. The existence of breakaway S/R values for the four- and six-fin configurations is a result of the "zone of silence" present in supersonic flow ahead of a shock wave. For example, with the four-fin configuration at positive sideslip, the flow around the horizontal fins is not affected by the vertical fins until the shock waves intersect the fin plane. The accompanying pressure differences significantly alter the K_ϕ results beyond the intersection line; however, at smaller values of S/R, K_ϕ is unaffected by the number of fins. It is interesting to note that although the pressure differences caused by shock waves and expansion fans are opposite in nature, they

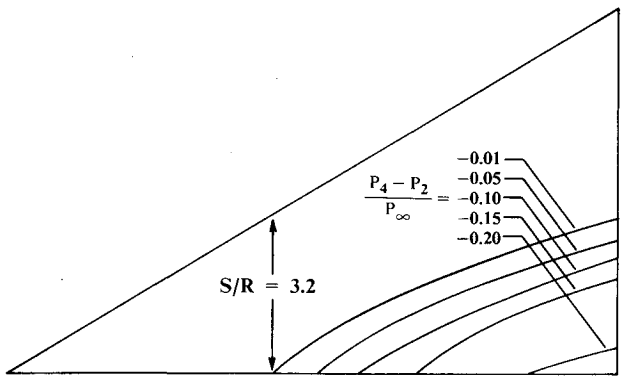

a) Bottom surface, $\beta = -3$ deg

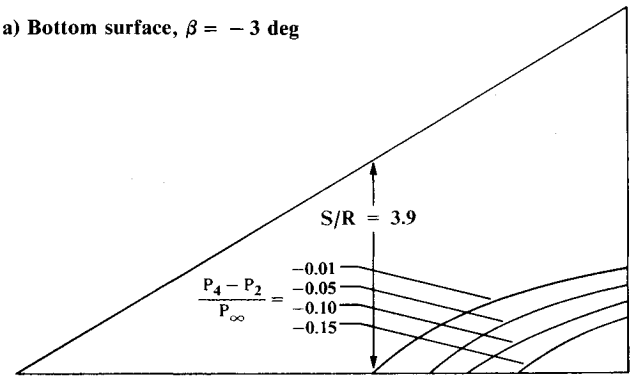

b) Top surface, $\beta = -3$ deg

Fig. 19 Contour plot of fin pressure differences between four- (P_4) and two- (P_2) fin cases at $M_\infty = 3.5$, $\alpha = 3$ deg, $\epsilon = 31.0$ deg, and $\beta = -3$ deg.

produce K_ϕ values that are not strongly dependent on whether the sideslip angle is positive (producing shock waves) or negative (producing expansion fans).

The breakaway values of S/R for the six-fin configuration are lower than those for the four-fin configuration due to the proximity of the fins. The angular separation between fins is only 60 deg for the six-fin configuration compared to 90 deg for the four-fin configuration. This allows shock waves and expansion fans that form on adjacent fins to intersect the fin of interest at lower values of S/R. A similar argument can be used to show that the 120 deg angular separation in the three-fin configuration is large enough to prevent the shock waves and expansion fans from affecting the K_ϕ results for $S/R < 6$. This also implies that the breakaway S/R value for a five-fin configuration will fall somewhere between the breakaway points for the four- and six-fin configurations.

Finally, the trend of increasing breakaway values of S/R with increasing M_∞ and ϵ can be explained by recalling that increases in either M_∞ or ϵ increase the Mach number normal to the leading edge of each fin on the missile. This causes the angle between the fin and shock wave or expansion fan to decrease. Consequently, the line of intersection of shock waves or expansion fans from adjacent fins moves farther aft on the fin of interest.

The breakaway values of S/R predicted by SWINT are consistent with linear theory. Equation (D-3) in Ref. 18 states that the onset of fin-fin interference will occur at

$$S/R = 1 + \theta B \tan\epsilon \tag{8}$$

where θ represents the angular separation in radians between adjacent fins. Inspection of Eq. (8) shows that the effects of the number of fins, Mach number, and semivertex angle on the breakaway points are the same as those just described. In addition, Eq. (8) agrees fairly well with the SWINT predictions for the breakaway values of S/R shown in Figs. 13 and 16.

Conclusions and Recommendations

Values of K_ϕ for two-, three-, four-, and six-fin missile configurations have been determined for values of S/R ranging from 1-6 using a finite-difference Euler code. It is shown that K_ϕ is sensitive to changes in M_∞, ϵ, and β in addition to the number of fins and S/R as predicted by slender body theory. The K_ϕ values were compared to the SBT results for two- and four-fin missile configurations. The results are similar in magnitude, but differ in trend when changing from two- to four-fin configurations. Fin pressure distributions were analyzed to show that the formation of fin shock waves and expansion fans influence K_ϕ for missiles with four and six fins. The breakaway values of S/R and inflection points in the K_ϕ curves are shown to be directly related to the position of the shock waves and expansion fans originating from the adjacent fins. The research also indicates that K_ϕ results can change dramatically if the fins are located in the vicinity of the missile nose or other areas where large body pressure gradients are present.

The utility of the equivalent angle-of-attack method depends on the ease with which the interference factors contained therein can be determined. The simple SBT formulas for $K_{W(B)}$ and K_ϕ are thus well suited to this method. This study, however, indicates that K_ϕ is a function of missile flight conditions and various geometric parameters, and these dependencies are a result of the shock waves and expansion fans present in the flowfield. SBT does not directly account for these phenomena; thus, the missile designer should be aware of the limitations of using SBT values for the interference factors in the equivalent angle-of-attack method when experimental or numerical values are not available.

In the future, these K_ϕ results should be extended to include higher angles of attack and sideslip, and a wider range of Mach numbers. Also, investigation of different fin planforms and fins with subsonic leading edges is needed to extend the applicability of K_ϕ to more missile geometries and flight conditions.

Acknowledgment

This work was supported by McDonnell Douglas Astronautics Company, St. Louis, Missouri, through the Independent Research and Development program, monitored by John E. Williams. Additional funds were provided by the Missouri Research Assistance Act.

References

[1]Agnone, A. M., "Supersonic Flow Over a Cruciform Configuration at Angle of Attack," *Journal of Spacecraft and Rockets,* Vol. 23, Sept.-Oct. 1986, pp. 451-452.

[2]Larson, E. S., "Normal Force Characteristics at Supersonic Speeds of Sharp Edged Delta Wings," AIAA Paper 87-0214, 1987.

[3]Spreiter, J. R. and Sacks, A. H., "A Theoretical Study of the Aerodynamics of Slender Cruciform-Wing Arrangements and Their Wakes," NACA Rept. 1296, 1957.

[4]Shang, J. S. and Scherr, S. J., "Navier-Stokes Solution of the Flow Field Around a Complete Aircraft," AIAA Paper 85-1509, 1985.

[5]Wardlaw, A. B., Baltakis, F. P., Martin, F. M., Priolo, F. J., and Jettmar, R. U., "A Godunov Method for Supersonic Tactical Missiles," *Journal of Spacecraft and Rockets,* Vol. 24, Jan.-Feb. 1987, pp. 40-47.

[6]Vukelich, S. R. and Jenkins, J. E., "Missile DATCOM: Aerodynamic Prediction of Conventional Missiles Using Component Build-Up Techniques," AIAA Paper 84-0388, 1985.

[7]Vukelich, S. R. and Jenkins, J. E., "Evaluation of Component Build-Up Methods for Missile Aerodynamic Predictions," *Journal of Spacecraft and Rockets,* Vol. 19, Nov.-Dec. 1982, pp. 481-488.

[8]Stoy, S. L. and Vukelich, S. R., "Prediction of Aerodynamic Characteristics of Unconventional Missile Configurations Using Component Build-Up Methods," AIAA Paper 86-0489, 1986.

[9]Hemsch, M. J. and Nielsen, J. N., "Equivalent Angle-of-Attack Method for Estimating Nonlinear Aerodynamics of Missile Fins," *Journal of Spacecraft and Rockets,* Vol. 20, July-Aug. 1983, pp. 356-362.

[10]Hemsch, M. J. and Nielsen, J. N., "Extension of Equivalent Angle of Attack Method for Nonlinear Flowfields," *Journal of Spacecraft and Rockets,* Vol. 22, May–June 1985, pp. 304–308.

[11]Stoy, S. L. and Vukelich, S. R., "Extension of the Equivalent Angle-of-Attack Prediction Method," AIAA Paper 84-0311, 1984.

[12]Nielsen, J. N., *Missile Aerodynamics,* McGraw-Hill, New York, 1960, pp. 125–129.

[13]Ashley, H. and Landahl, M. T., *Aerodynamics of Wings and Bodies,* Addison-Wesley, Reading, MA, 1965.

[14]Wardlaw, A. B., Baltakis, F. P., and Solomon, J. M., "An Inviscid Computational Method for Tactical Missile Configurations," NSWC TR 81-457, Dec. 1981.

[15]Wardlaw, A. B., Baltakis, F. P., and Solomon, J. M., "Supersonic Inviscid Flowfield Computations of Missile Type Bodies," *AIAA Journal,* Vol. 19, July 1981, pp. 899–906.

[16]Priolo, F. J. and Wardlaw, A. B., "A Comparison of Inviscid Computational Methods for Supersonic Tactical Missiles," AIAA Paper 87-0113, 1987.

[17]Jenn, A. A., "Numerical Determination of Missile Aerodynamic Interference Factors," M.S. Thesis, Dept. of Mechanical and Aerospace Engineering, Univ. of Missouri–Rolla, Rolla, MO, Dec. 1987.

[18]Nielsen, J. N., Hemsch, M. J., and Smith, C. A., "A Preliminary Method for Calculating the Aerodynamic Characteristics of Cruciform Missiles to High Angles of Attack Including Effects of Roll Angle and Control Deflections, ONR Rept. CR215-226-4F, 1977.